Tracking Single Secretory Granules in Live Chromaffin Cells by Evanescent-Field Fluorescence Microscopy

J. A. Steyer and W. Almers
Max-Planck-Institut für Medizinische Forschung, 69120 Heidelberg, Germany

ABSTRACT We have observed secretory granules beneath the plasma membrane of chromaffin cells. Using evanescent-field excitation by epiillumination, we have illuminated a thin layer of cytosol where cells adhere to glass coverslips. Up to 600 frames could be recorded at diffraction-limited resolution without appreciable photodynamic damage. We localized single granules with an uncertainty of ~30 nm and tracked their motion in three dimensions. Granules in resting cells wander randomly as if imprisoned in a cage that leaves ~70 nm space around a granule. The "cage" itself moves only slowly ($D = 2 \times 10^{-12}$ cm^2/s). Rarely do granules arrive at or depart from the plasma membrane of resting cells. Stimulation increases lateral motion only slightly. After the plasma membrane has been depleted of granules by exocytosis, fresh granules can be seen to approach it at an angle. The method will be useful for exploring the molecular steps preceding exocytosis at the level of single granules.

INTRODUCTION

Endocrine cells release transmitters and hormones by exocytosis of secretory vesicles or granules. To become available for exocytosis, granules must move from the cytosol to the plasma membrane and dock there. In chromaffin as in other cells, a layer of filamentous actin covers the internal side of the plasma membrane. In electron micrographs, this "cortical" actin layer appears to be dense enough to be a barrier to granules on their way to the plasma membrane (Nakata and Hirokawa, 1992). Not surprisingly, filamentous actin greatly reduces the mobility of isolated chromaffin granules in dynamic light-scattering studies in vitro (Miyamoto et al., 1993). Indeed, some studies have suggested that cortical actin is a negative regulator of secretion that is partially and transiently degraded when actin-severing enzymes become activated during stimulation (see Trifaró and Vitale, 1993, for a review). However, a restriction of granule movement beneath the plasma membrane has never been demonstrated. Indeed, some studies suggest instead that actin filaments provide tracks along which granules are propelled by myosin molecules (Kumakura et al., 1994; Bi et al., 1997; Terrian and Prekeris, 1997). Whether cortical actin helps or hinders the motion of granules to the plasma membrane remains unresolved; indeed, little direct information is available on how granules move beneath the plasma membrane.

It would be of interest to observe single granules near the plasma membrane in live chromaffin cells, either by differential interference contrast (Terakawa et al., 1991) or by fluorescence microscopy. Confocal fluorescence microscopy has provided valuable information on the turnover of synaptic vesicles (Betz and Angleson, 1998) and chromaffin granules (Smith and Betz, 1996) and may seem especially attractive for such studies. However, this method imposes a high radiation burden on cells, as the entire cell is illuminated with fluorescence excitation light, whereas most fluorescence emission is rejected at the confocal pinhole. An alternative is to illuminate selectively a thin layer of cytosol beneath the plasma membrane and then collect all fluorescence emission reaching the microscope objective. This can be done by total internal reflection microscopy (Axelrod et al., 1992) when chromaffin cells adhere to a glass coverslip. Total internal reflection at the cytosol/glass interface sets up an evanescent field in the cytosol. Declining with distance from the glass, the evanescent field excites fluorescence in granules in proportion to their proximity to the plasma membrane. Evanescent-field microscopy may therefore allow one to track granules with excellent resolution, also in a direction vertical to the plasma membrane. The technique could complement an earlier approach for vertical tracking (Kao and Verkman, 1994).

Indeed, single granules made fluorescent with green fluorescent protein (Lang et al., 1997) or acridine orange (Steyer et al., 1997; Oheim et al., 1998) are readily observed with total internal reflection microscopy in living cells. Here we evaluate a convenient method that uses a high numerical aperture objective to both generate an evanescent field by epiillumination and observe the fluorescence emitted therein (Stout and Axelrod, 1989). The method allowed us to track single chromaffin granules beneath the plasma membrane in three dimensions and to analyze their motion by methods previously used with individual molecular complexes in cellular compartments (Qian et al., 1991; Kusumi et al., 1993; Ghosh and Webb, 1994; Saxton and Jacobson, 1997). Granules beneath the plasma membrane were found to move as if imprisoned in a cage, and most were prevented from moving long distances. Our results provide direct evidence that subplasmalemmal granules are restricted in

Received for publication 17 August 1998 and in final form 15 December 1998.

Address reprint requests to Dr. Wolfhard Almers, Max-Planck-Institut für Medizinische Forschung, 69120 Heidelberg, Jahnstrasse 29, Germany. Tel.: 49-6221-486-350; Fax: 49-6221-486-325; E-mail: almers@mzf.mpimf-heidelberg.mpg.de.

The authors' present address is Vollum Institute, 3181 S.W. Sam Jackson Park Road L474, Portland, OR 97201-3098.

0006-3495/99/04/2262/10 $2.00

their mobility. Membrane-resident granules exchange only slowly with those deeper in the cytosol, and even severe stimulation causes only a slight increase in mobility.

MATERIALS AND METHODS

Cell preparation and granule labeling

Bovine chromaffin cells were prepared as described (Parsons et al., 1995), plated on poly-D-lysine (0.5 mg/ml)-coated glass coverslips, and used 2 or 3 days after plating. Their secretory granules were labeled by incubating the cells in a buffer containing 3 μM acridine orange (15 min, 21 $\pm$ 1°C) and then washing the cells twice in dye-free buffer. The buffer contained (in mM) 135 NaCl, 2 KCl, 5 $CaCl_2$, 2 $MgCl_2$, 4 mg/mL glucose, 10 Na-HEPES (pH 7.2). Acridine orange is a weak base that accumulates in acidic compartments such as chromaffin granules. PC-12 cells were grown as described (Lang et al., 1997) and used without stain.

After washing, the coverslip was inserted into the sample chamber (POC; Bachhofer, Reutlingen, Germany), and the chamber was rigidly secured to the mechanical stage (SCAN IM 100 × 100; Märzhäuser, Wetzlar, Germany) of a modified Zeiss-Axiovert 135 microscope (see later). Cells were viewed at first in reflection interference contrast (RIC) mode with illumination at 600 nm, a wavelength not significantly absorbed by acridine orange. Adherent cells were chosen; they were apparent by their dark image ("footprint") in RIC. The focal position where the contours of the "footprint" appeared sharpest was taken as a reference. After selecting a cell and focusing on it in RIC, we moved the objective lens 300 nm upward, using a calibrated piezoelectric drive. This distance was determined to be the focal shift between the RIC plane (λ = 600 nm) and the plane through the center of a 280-nm fluorescent bead (λ_{em} = 500 nm) directly adsorbed to the glass coverslip. With this procedure, cells could be selected and the granules near the plasma membrane brought into focus without exposing the cells to fluorescence excitation light (488 nm). The experiment could now start, using excitation light applied through a computer-driven shutter while images were being recorded by our camera. Exposure to 488-nm light at other times was avoided. All experiments were performed at 22–25°C; values are given $\pm$ SEM.

To stimulate secretion, we raised $[K^+]$ in the bath by local perfusion. The openings of two flexible glass tubes (75 μm inner, 144 μm outer diameter, MicroFil; World Precision Instruments) glued together at their tips were brought within 200 μm of the cell. Bath solution flowed through one tube continuously except when stimulation buffer was applied through the other. The stimulation buffer contained (in mM) 75 NaCl, 62 KCl, 5 $CaCl_2$, 2 $MgCl_2$, 4 mg/ml glucose, and 10 HEPES (pH 7.2) unless indicated otherwise. The elevated $[K^+]$ made the plasma membrane potential more positive, opened voltage-gated Ca channels, and raised cytosolic $[Ca^{2+}]$ (probably to ~2–2.7 μM; Plattner et al., 1997). After 2 min at raised $[K^+]$, standard solution was reapplied. The perfusion system exchanged solution within ~3 s, as measured by application of norepinephrine to the tip of an amperometric carbon fiber placed at the same position as the cell.

For calibration purposes we also viewed green fluorescent beads (280 nm diameter; excitation 490 nm, emission 510 nm) modified with surface carboxylate groups (Molecular Probes, Eugene, OR). The diameter was chosen because it was similar to that of chromaffin granules (330 nm, Parsons et al., 1995; 360 nm, Plattner et al., 1997).

Prismless evanescent-field microscope

Cells adhering to a glass coverslip were excited by the evanescent field set up by total internal reflection of a laser beam at the glass-cell interface. Total internal reflection was achieved by applying the beam through a 1.4 NA objective (Planapochromat 100×, 1.4 N.A.; Zeiss, Germany) that was also used for observation ("prismless" total internal reflection; Stout and Axelrod, 1989; Conibear and Bagshaw, 1996). The setup is based on a modified inverted microscope (Axiovert 135 TV, Zeiss); this is illustrated in Fig. 1.

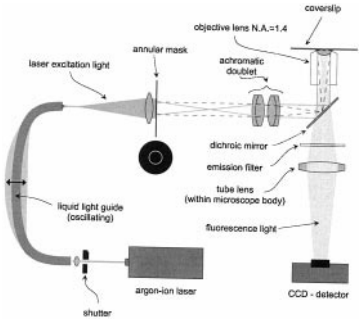

FIGURE 1 Schematic setup of the evanescent-field microscope. The objective, the dichroic mirror, the emission filter, and the tube lens are components of the regular inverted microscope. See text for details.

Light from a 4-W argon laser (2020–4S; Spectra Physics) was passed through a software-controlled shutter (Uniblitz; Vincent Associates, Rochester, NY) that opened only during camera exposure. The 488-nm argon line (generally ~100 mW) was focused into one end of a 2-m-long, 2-mm-diameter liquid light guide (Dr. Rapp Optoelektronik, Hamburg, Germany). The other end of the light guide was fixed to an optical rail system (Spindler and Hoyer) aligned with the epifluorescence port of the microscope. A lens of 50.2 mm focal length formed a real image of the planar surface of the light guide at a plane between the annulus and an achromatic doublet that was conjugate to the specimen plane ("critical illumination"). This images the end of the light guide onto the specimen plane. Use of the light guide had two advantages. First, it allowed us to place the laser and microscope on different tables and avoided the transmission of laser vibrations to the microscope. Second, its end formed a uniformly luminous object for even illumination of the specimen. The fiber was vibrated so that any interference patterns ("speckles") moved rapidly and were canceled by averaging during the exposure time of a single frame.

The beam passed next through an annular mask (4.3 mm inner and 4.5 mm outer diameter), blocking all but the most peripheral rays from passing the back focal plane of the objective. The annulus was cut into 20-μm-thick stainless steel foil, glued to a glass coverslip, and held by an *x-y* translator for alignment to the optical axis. A pair of achromatic doublets (each with a 160-mm focal length) imaged the mask with a nearly 1:1 conjugate ratio onto the back focal plane of the objective lens. There the annulus ensured that rays leave the objective only above a critical angle and are thus totally reflected at the glass-water or glass-cell interface.

The iris diaphragm, focusing lens, filter holder, and excitation filter normally present in the epifluorescence port were removed. A dichroic mirror (505DRLP02; Omega Optical) reflected the excitation light into the objective lens and transmitted emitted fluorescence light (at 540 nm) to the cameras. Excitation light reflected back into the objective was prevented from reaching the camera by the dichroic mirrors and an emission filter (OG530; Omega Optical).

A second dichroic mirror (620DRLP02; Omega Optical) was placed between the annulus and the achromatic doublet to couple two other modes of illumination into the epifluorescence port. First, it partially reflected blue light (474–496-nm bandpass, 485DT22; Omega Optical) from a halogen lamp (12 V, 100 W; Zeiss Co.) for normal epifluorescence excitation. Second, it reflected red light (600-nm bandpass) from a second halogen lamp to image the "footprint" made by the cell on the glass substrate in reflection interference contrast (RIC). In this observation mode, abundant stray light is reflected into the objective. To cancel it, we subtracted from the RIC image of each cell an image from an area showing no cell. With the 14-bit dynamic range of a slow-scan CCD camera, this yielded a RIC image of the cell with adequate contrast. Electronic shutters selected between brightfield, epifluorescence, RIC, and evanescent-field illumination.

For the first hour after the experimental chamber was inserted into our inverted microscope, the distance between the stage and the objective changed by some 40 nm/min, causing the image to drift out of focus during continuous observation. This drift was reduced to ~3 nm/min by mounting

the objective on a calibrated piezoelectric drive (PIFOC P-721.10; Physik Instrumente, Waldbronn, Germany). The distance between stage and objective was measured by an inductive position sensor (E-115.21; Physik Instrumente; rated accuracy 10 nm) and was held constant by raising or lowering the objective using feedback electronics (E509.L1; Physik Instrumente). The arrangement also allowed calibrated movements of the objective up and down by application of the appropriate analog voltages. We assumed the focal plane to move 88% of the distance moved by the objective. This allows for the difference in refractive index between water and the immersion oil (Majlof and Forsgren, 1993). All vertical distance measurements were corrected accordingly.

Image collection

Fluorescent light was collected through the bottom port of the inverted microscope. In most experiments, images were recorded through an image intensifier (VS3–1845; VideoScope International Ltd.) and a video camera (CCDC72; Dage MTI) and stored on an optical memory disc recorder (OMDR, TQ-3038F; Panasonic). The quantum efficiency of the image intensifier reached ~25% at 500 nm. Custom electronics ensured that the shutter opened only during image acquisition. In some experiments, frames were acquired at 30 Hz in bursts of 200 frames. In others, the fluorescent photons collected during 110-ms light exposures were integrated on the video chip, and the resulting image was written to the OMDR at 1–2-s intervals. Laser illumination intensity was set to avoid saturation while maximizing the dynamic range (8 bits) of the video camera. Images were later played into the computer at 50 nm/pixel through a frame grabber (Image-LC; Matrox Electronic Systems) and analyzed with the MetaMorph software package (Universal Imaging Co., West Chester, PA).

Occasionally, we used a slow-scan air-cooled CCD-camera with a 14-bit A/D-converter (ST-138S; Princeton Instruments). The back-illuminated chip (SI502BA; SITe) had 512 × 512 pixels of 24 × 24 μm^2 each; its quantum efficiency exceeded 70% at 500–750 nm. To avoid spatial undersampling by the large pixels, the fluorescence image was magnified (Optovar magnifying lens, 2.5×). The camera was controlled and coordinated by a PC computer running MetaMorph under MS Windows 3.11. Stacks of 100–200 images were taken at 0.5 Hz.

Analysis of lateral granule position

To quantify the mobility of granules parallel to the plasma membrane, we measured their position using software modules provided by MetaMorph. First, each stack of images was processed by a median (long-pass) filter at a spatial frequency corresponding to $1/\mu m$. The resulting stack contained what may be called the local background of the stained cell; it was subtracted from the original to obtain a high-pass filtered stack of images. For tracking, we selected the brightest granules that did not collide with neighboring granules during the recording period; up to eight granules were selected in each cell. A binary version of the stack was calculated using a threshold brightness chosen to keep the granule of interest separate from its neighbors, yet keeping its binary image as large as possible. The binary stack was used as a mask that caused all pixels below threshold to be set to zero. The algorithm also found regions of fewer than five nonzero contiguous pixels and set them to zero as well. This pixel selection identified a single contiguous region as the image of a granule. The exact location of the granule was determined as the center of mass of the fluorescence within the region defined by each granule's mask. The granule's x and y coordinates thus determined in each frame were saved in a file for subsequent analysis.

For each granule trajectory the mean square displacement (MSD) in the plane of the membrane was calculated as follows. Assume images are taken at time intervals δt. Let $x(t)$ and $y(t)$ be the coordinates of the granule in one image, and let $x(t + n\delta t)$ and $y(t + n\delta t)$ be those in another image taken $n\delta t$ later. Then the square of the displacement during $n\delta t$ is $[x(t + n\delta t) - x(t)]^2 + [y(t + n\delta t) - y(t)]^2$. Generally, for a given interval $n\delta t$, the MSD is (Qian et al., 1991)

$$\mathrm{MSD}(n\delta t) = \frac{1}{N-n}\sum_{j=1}^{N-n}\{[x(j\delta t + n\delta t) - x(j\delta t)]^2 + [y(j\delta t + n\delta t) - y(j\delta t)]^2\} \quad (1)$$

where N is the total number of images in the recording sequence and n and j are positive integers with $n = 1, 2, \ldots (N - 1)$. The granule's coordinates at time $j\delta t$ are $(x(j\delta t),y(j\delta t))$, and those a time interval $n\delta t$ later are $(x(j\delta t + n\delta t),y(j\delta t + n\delta t))$.

RESULTS

Depth of illuminated layer

Our aim was to use evanescent-field illumination to selectively excite a thin layer of cytosol where a cell adhered to a coverslip. To determine the thickness of the illuminated layer in vitro, fluorescent beads were adsorbed to the coverslip and to a lens placed on it curved side down (Fig. 2 *A*). We viewed the beads in a saline containing 15% bovine serum albumin (BSA) to approach the refractive index of cytosol. Adding the BSA strongly diminished the contrast of cultured fibroblasts under phase-contrast optics. We selected a field of view containing solitary beads, some adhering to the coverslip and others to the lens. Using a calibrated piezoelectric drive, we moved the objective upward in 50-nm steps, watching beads as they came into and then went out of focus. At each vertical plane, images were taken with both epifluorescence and evanescent-field excitation. To test for photobleaching, the experiment was concluded with repeat images taken at the first (lowest) vertical position.

The fluorescence from several beads was followed through all vertical positions. Beads brightened as they came into focus, then dimmed again as the focal plane moved beyond them. Plotting fluorescence intensity against the vertical distance of the focus defines the vertical position of each bead. Fig. 2, *B* and *C*, shows results from two beads. The left profile apparently was from a bead adsorbed to the coverslip because the bead came into focus at the same vertical plane as several other beads in the field of view. In contrast, the bead that gave the rightmost profile was at some distance from the coverslip, presumably because it had adsorbed to the lens. With epifluorescence, the two beads were about equally bright (Fig. 2 *B*). With evanescent excitation (Fig. 2 *C*) the remote bead appeared dimmer, reflecting the weaker evanescent field at that distance. Peak intensity ratios (evanescent field/epifluorescence) were plotted against vertical distances in Fig. 2 *G* (*circles*). Results were well described by an exponential function whose decline (*e*-fold in 185 nm, *dashed line*) reflects the decay of the evanescent field. During an actual experiment, the objective does not move but remains focused on the granules closest to the coverslip. To mimic this, we measured the fluorescence intensity in a plane focused at the center of a granule adhering to the coverslip and plotted it

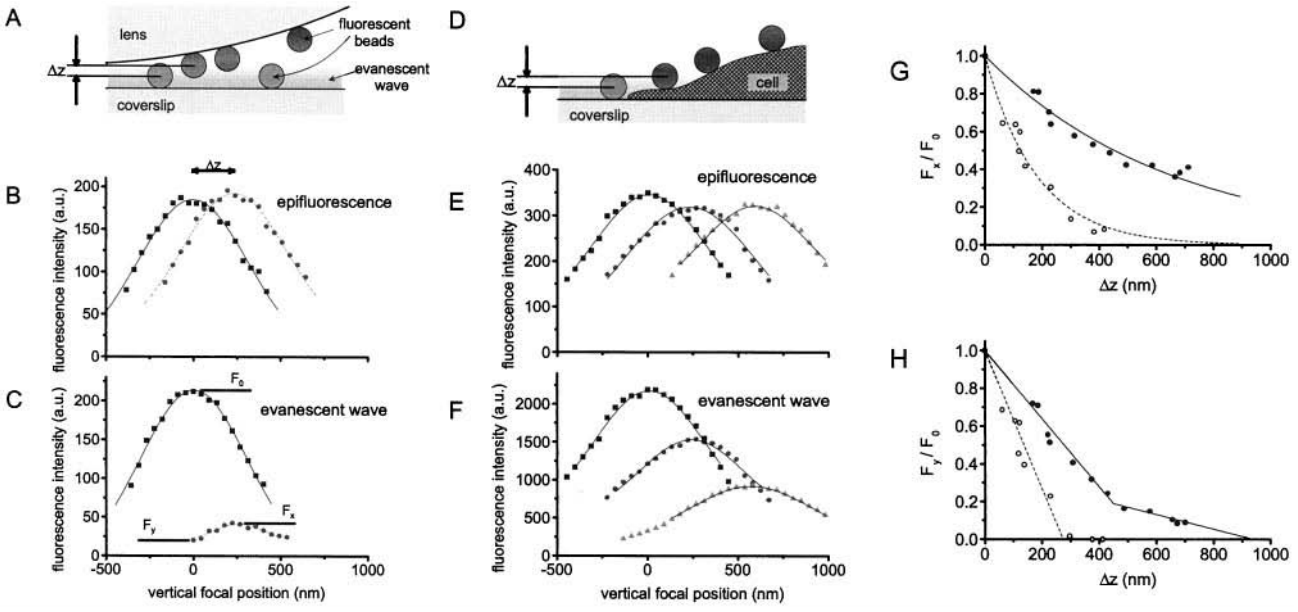

FIGURE 2 Depth calibration of the evanescent field. (A) In vitro calibration. A plano-convex lens was placed on the coverslip curved side down. Green fluorescent beads (280 nm diameter) were suspended in PBS containing 15% BSA. One hundred microliters of the suspension was placed at the contact region of the coverslip and lens (22 mm diameter, 40 mm focal length) so that beads were adsorbed to the surfaces of both. (*B* and *C*) Fluorescence intensity (arbitrary units) against vertical distance, for two beads. One touched the coverslip (*left profile*) while the other was held at some distance, presumably because it had bound to the lens surface. Lines show a Gaussian fitted to the top 60% of each curve. The distance between the two peaks of the Gaussian curves corresponds to the distance between the centers of the beads and hence to the distance of the remote bead from the coverslip. The fluorescence intensity is the average in a circle of 300 nm superimposed on the brightest region of the image of each bead. (*B*) With epifluorescence. (*C*) With evanescent-field illumination. (*D*) Experiment as in *A*, with beads adsorbed both to coverslips and to the top surfaces of four PC-12 cells. (*E* and *F*) Analogous to *B* and *C*. Fluorescence intensity was plotted against vertical focal distance for three granules viewed with epifluorescence (*E*) or evanescent field excitation (*F*). The leftmost granule was located in a region not covered by a cell, as verified in the interference reflection contrast image (not shown). Hence it had adsorbed to the coverslip. (*G*) Fluorescence intensity ratios (F_x/F_0) of beads as a function of their distance from beads adsorbed to the coverslip. Fluorescence values are the maxima of the fitted Gaussians and represent values obtained for each bead at the vertical position where it is brightest. Open circles from *B* and *C*: The exponential function declines *e*-fold in 185 nm (*dashed curve*). Filled circles from *E* and *F*: The exponential declines *e*-fold in 646 nm (*continuous curve*). (*H*) Fluorescence intensity normalized as in *G*, but measured at the fixed focal plane where beads adsorbed to the coverslip appear brightest. Open circles from *B* and *C*: the regression line (*dashed curve*) intercepts the abscissa at 274 nm. Filled circles from *E* and *F*: these were approximated by two regression lines (*continuous curve*) as follows. For $\Delta z < 450$ nm, $F = 1 - (1/555\text{ nm}) \times \Delta z$; for $\Delta z > 450$ nm, $F = 0.363 - (1/2588\text{ nm}) \times \Delta z$. *F* is the fluorescence ratio, and Δz is the vertical coordinate as defined in *A*. The two continuous curves were used later to calculate changes in the vertical position of chromaffin granules from their changes in fluorescence.

against the distance of each bead. The plot is well fitted by a straight line intersecting the abscissa at 274 nm (Fig. 2 *H*, *dashed*). The decline with distance reflects the decay of the evanescent field as well as the bead going out of focus.

For an in vivo determination, fluorescent beads were sprinkled onto a coverslip covered sparingly with adherent PC-12 cells. Some beads fell on the glass, others on the margins of cells. Vertical scans were made as above to explore beads lying on the coverslip and others that were separated from the coverslip by cytosol of varying thickness (four different cells; Fig. 2 *D*). Intensity ratios obtained with evanescent-field and epifluorescence excitation were plotted against the vertical distance of each bead in Fig. 2 *E*. Compared with in vitro measurements, peak intensity falls more gently with distance (Fig. 2 *G*, *continuous curve*), indicating a wider spread of the evanescent field. At least part of the difference may be explained if large scattering particles, such as organelles, cause some evanescent light to become propagated. Fig. 2 *H* (*continuous curves*) plots intensity ratios of beads against their distance, measured with the focal plane fixed at the center of beads on the coverslip. We will use these data later to convert intensity fluctuations of granules into vertical movements; we fitted them by two straight line segments for that purpose (see legend of Fig. 2). Although the calibration is likely to be of limited accuracy, Fig. 2 *H* (*continuous curve*) is more appropriate than the dashed line for locating granules within cells.

Single granules viewed in resting cells

Fig. 3 shows micrographs of a single adherent chromaffin cell viewed in brightfield, epifluorescence, and evanescent-field excitation. With epifluorescence the cell fluoresces nearly uniformly (Fig. 3 *B*), whereas evanescent-field excitation revealed single fluorescent spots (Fig. 3 *C*) superimposed on a background haze, probably representing out-of-focus granules deeper within the cell. The fluorescent area is smaller than with epifluorescence because the region where the cell adheres to the glass is smaller than the cell's

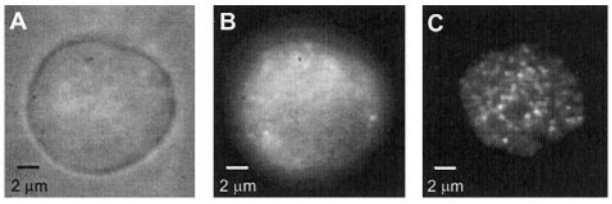

FIGURE 3 Chromaffin cell with three imaging methods. (*A*) Brightfield image. (*B*) Epifluorescence image. (*C*) Evanescent-field image at the same focal position as in *B*.

horizontal projection. This was also verified by comparing the brightfield image with the interference reflection image (not shown). The density of fluorescent spots in Fig. 3 *C* ($1.41/\mu m^2$) was typical for our cells (average 1.31 ± 0.04 granules/μm^2, $n = 31$ cells). Fluorescent spots almost certainly represent single chromaffin granules, as many of them are lost in a Ca-dependent manner when cells are stimulated to secrete (Steyer et al., 1997; Oheim et al., 1998). High-pass filtering eliminates most of the local background (see Fig. 4).

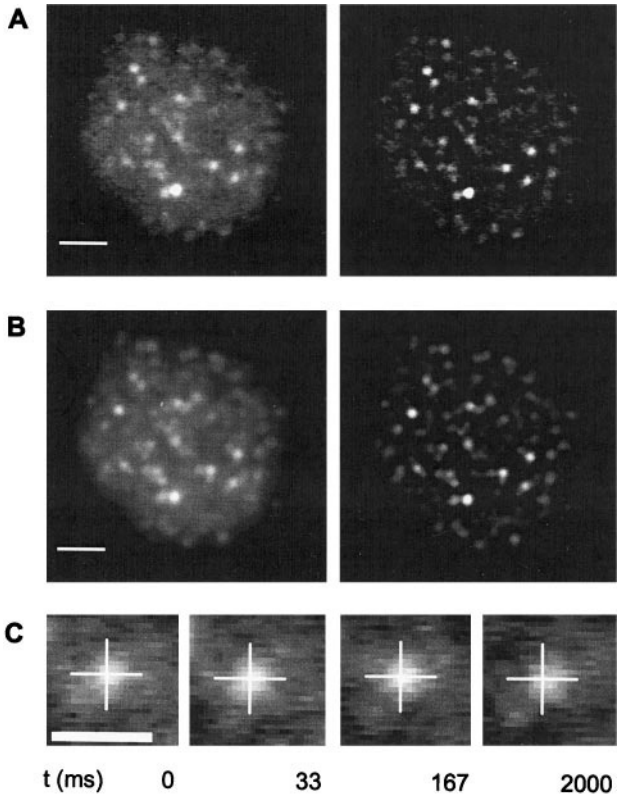

FIGURE 4 Granules in a chromaffin cell move little. (*A*) First image in a stack of 200 taken at 33-ms intervals. (*B*) Average of the entire stack. (*A* and *B*) Unfiltered (*left*) and high-pass filtered (*right*) images. For filtering, blurred versions of images on the left were first generated by low-pass filtering at a spatial frequency of 1 μm (see Materials and Methods). Subtraction of the blurred from the original images yielded the images on the right. (*C*) A single granule was magnified. Its first, second, and later images in the stack are shown. Calibration bars: 2 μm in *A* and *B* and 1 μm in *C*.

Mobility of granules in the plane of the plasma membrane

To analyze granule motion, unstimulated chromaffin cells were imaged with evanescent-field excitation for 6.7 s at 30 Hz. Fig. 4 *A* shows the first image in a stack of 200, and Fig. 4 *B* shows the average of the entire stack. Unfiltered (*left*) and high-pass filtered (*right*) images are shown. Fig. 4, *A* and *B*, shows subtle differences, probably reflecting vertical motion of some granules. For example, some of the brightest granules in *A* are comparatively dim in *B* and vice versa, and some granules visible in *A* are missing in *B*. On the whole, however, the two pairs of images are nearly identical, and hence most granules moved little over the 6.7-s interval explored. In cells observed for longer durations, single granules occasionally traveled distances of >1 μm at a top speed of 0.26 μm/s in one instance, but such cases were rare (less than one granule per cell per minute) and were excluded from further analysis. Fig. 4 *C* shows magnified versions of one of the granules in Fig. 4, *A* and *B*, at different times during the observation period. Although little movement is apparent in the images, viewing the movie showed that the granule wandered slightly around a resting position.

Fig. 5 *A* plots the *x* and *y* coordinates of the granule in Fig. 4 *C* against time. The traces show apparently random motion. For analysis, we measured the square of the distance traveled by a granule during various time intervals and plotted the MSD against the time interval (Fig. 5 *B*, *filled circles*). If granules moved randomly and with a single diffusion coefficient, the plot should yield a straight line whose slope is proportional to the diffusion coefficient. Instead, the plot shows downward curvature. Clearly, a single diffusion coefficient is insufficient to describe the motion observed.

The motion in Fig. 5 *B* did not result from instrument noise or drift, because an immobilized bead imaged with a similar signal-to-noise ratio (see legend to Fig. 5) showed only negligible displacements (*open squares* in Fig. 5 *B*). The average MSD was 0.00082 μm^2. Hence the uncertainty in our granule localization had an rms value of 0.03 μm. Movements smaller than this would have escaped detection in these experiments. The uncertainty would be less if more fluorescence were collected, e.g., during longer exposures or with stronger illumination.

To test for possible cell damage, we raised the external $[K^+]$ at the end of each experiment to stimulate secretion for 2 min. Exocytosis was seen to cause the sudden disappearance of single fluorescent spots (not shown; see Steyer et al., 1997). Of a total of 22 cells examined, only six were deficient in exocytosis, as they lost less than 20% of their fluorescent spots; these were excluded from further analysis. In one experiment, 600 exposures could be recorded while exocytosis remained intact. With a confocal microscope of comparable vertical resolution, fewer than 30 usable images could be obtained before clear signs of bleaching and photodamage became evident (not shown).

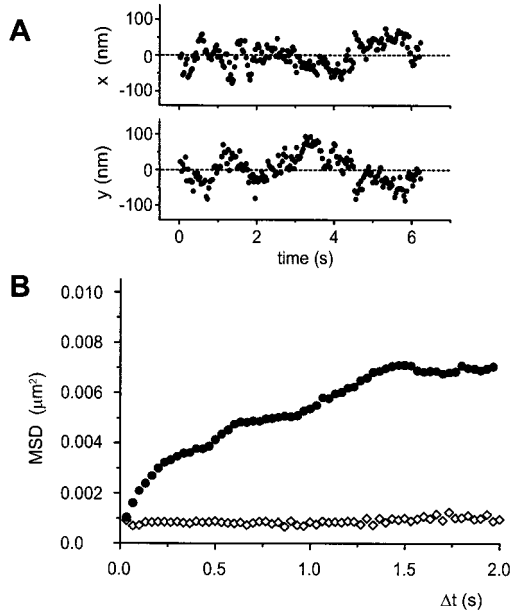

FIGURE 5 Rapid and random motions of a single granule. (*A*) Coordinates of a chromaffin granule against time (same granule as in *C*). (*B*) Mean square displacement (MSD) plotted against time interval Δt. To calculate the MSD we measured the distance moved over an interval of fixed duration, say 0.5 s, with the interval starting first at 0 ms after the beginning of the recording, then at 33 ms, then 66 ms, and so on until (6.700−0.5) s. All distances were squared. The average of all squared distances represents the MSD at 0.5 s. ●, Same granule as in *A*. ◇, Similar recordings from an immobilized bead (280 nm diameter) imaged at a signal-to-noise ratio (S/N) similar to that of the granule in *C*. To estimate the S/N of a granule or bead, we measured in high-pass filtered images the average brightness within the binary mask used to determine the lateral position of the granule or bead (see Materials and Methods). The S/N ratio was the brightness divided by its standard deviation with time. It was 17.2 for the bead and 16.6 for the granule.

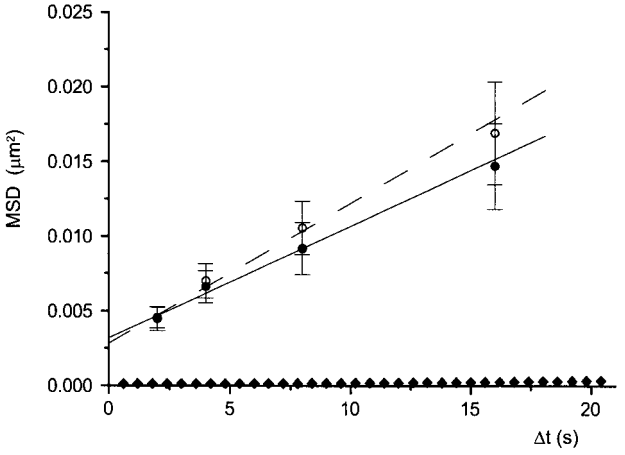

FIGURE 6 Motion of single granules from time-lapse recordings. Images were acquired every 2 s, first under resting conditions (1 min) and then for 2 min at elevated $[K^+]$. Each image was exposed for 110 ms, and light during that time was integrated on the chip of the video camera. The *x* and *y* coordinates of 18 granules from three cells were tracked as in Fig. 5, first for 1 min before and then for 1 min during stimulation. MSD plots were calculated from them; the average of the 18 plots is shown (± standard error). Before (●) and during (○) stimulation. The lines represent diffusion coefficients of 1.88×10^{-4} $\mu m^2/s$ in unstimulated cells (——) and 2.35×10^{-4} $\mu m^2/s$ during stimulation (– – –). ◆, Immobilized bead recorded at 2-s intervals for 5 min. Only three of seven cells examined were suitable for analysis. The others either detached, moved, or failed to perform sufficient exocytosis as they lost fewer than 20% of their granules within 2 min at elevated $[K^+]$. In the three cells a minority of 18 granules could be tracked for the entire duration of the experiment. The remainder either collided with other granules, were too dim, underwent exocytosis, or slowly faded away, presumably because they left the evanescent field.

Long-range motion and the effect of stimulation

Granule motion over longer times was explored in time-lapse recordings. Cells were imaged every 2 s, first under resting conditions (1 min) and then for 2 min in a saline solution where $[K^+]$ had been elevated to stimulate secretion. Eighteen granules in three cells were chosen for analysis. Stacks were processed and analyzed as in Fig. 5 to yield plots of MSD against time interval. Fig. 6 plots the average of all 18 plots, first at normal (*filled circles*) and then at elevated (*open circles*) $[K^+]$. The lines intersect the abscissa at MSD values ($\sim 30 \times 10^{-4}$ μm^2) that are larger than at $\Delta t = 0$ in Fig. 5 *B*. Evidently there is high-frequency motion in Fig. 5 *A* that is not resolved in our time-lapse recordings, but contributes to the MSD at all time intervals plotted. The plot reflects only the slower component of motion and does not significantly deviate from being linear. Apparently random motion with a single diffusion coefficient describes the data well on this time scale.

Diffusion coefficients were calculated individually for each unstimulated granule from its plot of MSD against time interval. Insofar as the motion explored is by diffusion with a single diffusion coefficient, each point may be assigned a variance, *V* (Qian et al., 1991):

$$V = (sn\Delta t)^2(2n^2 + 1)/(3n(N - n + 1)) \qquad (2)$$

Points were weighted by the reciprocal of their variance, and a regression line was fitted through them; *s* is the slope of the line. The diffusion coefficient *D* in unstimulated cells was calculated as $D = s/4$. The mean was $2.0 \pm 0.4 \times 10^{-4}$ $\mu m^2/s$ (three cells).

We calculated diffusion coefficients for each cell while $[K^+]$ was elevated and the cell was stimulated to secrete and determined the ratio of diffusion coefficients (stimulated/unstimulated). The ratio had a natural logarithm of 0.58 ± 0.29 ($n = 18$ granules in three cells), representing an 80% increase on stimulation. The difference is small but statistically significant ($p < 0.05$). We cannot rule out the possibility that it is partly a mechanical consequence of the exocytosis of neighboring granules.

To test for possible contributions from drift of the mechanical stage, we tracked the position of an immobilized, strongly illuminated bead for 5 min (*diamonds* in Fig. 6). If fitted by a straight line, the MSD plot would yield $D = 0.03 \times 10^{-4}$ $\mu m^2/s$. This may be considered our lower limit of detection.

Restricted diffusion of chromaffin granules

The granule of Figs. 4 and 5 apparently experienced random motion that could not be described by a single diffusion coefficient. This is confirmed in Fig. 7 (*open symbols*), where results from 13 granules in three cells are averaged. The plot clearly shows downward curvature.

This feature is reminiscent of diffusion in a cage, which can be described by the approximate equation (Saxton, 1993; Saxton and Jacobson, 1997)

$$\mathrm{MSD}(\Delta t) \approx R^2[1 - A_1\exp(-4A_2D_\alpha\Delta t/R^2)] \qquad (3)$$

Equation 3 represents the first two terms in an infinite series, and $A_1 = 0.99$ and $A_2 = 0.85$ are constant coefficients for the second term. R is the radius of the circular cage in which an infinitesimally small particle is free to diffuse with diffusion coefficient D_α. Applied to our situation, R is either the distance by which the radius of the cage exceeds that of a granule, or the length of a tether by which the granule is tied to a fixed point.

The MSD plot obtained for granules does not reach a horizontal asymptote (Fig. 6), as if the cage itself diffused with a finite but lower diffusion coefficient, D_β. To explore this idea quantitatively, we combined the data from video recordings (*open circles*) with those from time lapse recordings of Fig. 6 in unstimulated cells (*filled circles*). This was done by adding a constant to the data for unstimulated cells, chosen such that the two data sets coincided at an interval of 2 s (see figure legend). The plot in Fig. 7 was the result. It was fitted with a version of Eq. 3 that was expanded by a third term representing the relatively slower diffusion of the cage itself (diffusion coefficient D_β):

$$\mathrm{MSD}(\Delta t) \approx C + R^2[1 - A_1\exp(-4A_2D_\alpha\Delta t/R^2)] + 4D_\beta\Delta t \qquad (4)$$

$C = 5.3 \times 10^{-4}\ \mu\mathrm{m}^2$ is a constant that is included because the necessarily limited accuracy of our granule localization procedure creates an apparent displacement at all time intervals. The best fit was obtained with $R = (70 \pm 13)$ nm, $D_\alpha = (19 \pm 3) \times 10^{-4}\ \mu\mathrm{m}^2/\mathrm{s}$, and $D_\beta = (1.8 \pm 0.2) \times 10^{-4}\ \mu\mathrm{m}^2/\mathrm{s}$. Equation 4 is seen to provide a good fit. Evidently granules diffuse relatively freely for distances of ~70 nm, but ~10-fold more slowly over longer distances.

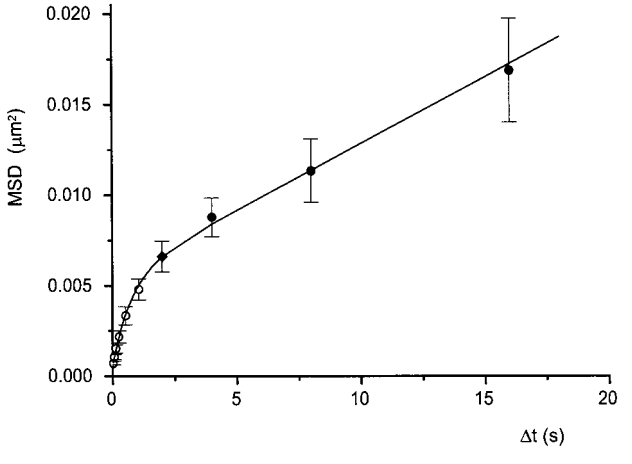

FIGURE 7 Two modes of diffusion. ○, Average MSD ± SE of 13 individual granule trajectories recorded at 30 frames/s. ●, Average MSD of 18 granule trajectories recorded at 0.5/s. Filled circles are from Fig. 6, but shifted upward by $21.6 \times 10^{-4}\ \mu\mathrm{m}^2$ to make the two data sets coincide at $\Delta t = 2$ s (◆). A minor portion of this upward shift ($6.3 \times 10^{-4}\ \mu\mathrm{m}^2$) would compensate for the fact that the exposure was 110 ms during time lapse and only 33 ms in video recordings. In Fig. 7, the MSD at 110 ms was $6.30 \times 10^{-4}\ \mu\mathrm{m}^2$ larger than at 33 ms. ——, Best least-squares fit of Eq. 4, with the data points weighted by the reciprocal of their variance. The fit parameters are given in the text.

Trajectories of granules approaching the plasma membrane

When chromaffin cells are stimulated to secrete, fluorescent granules disappear as they lose their dye due to exocytosis, and this depletes the plasma membrane of docked granules (Steyer et al., 1997; Oheim et al., 1998). New granules appear where previously none were visible, as granules move from the cytosol toward the plasma membrane. After stimulation has ended, fresh granules repopulate the membrane with a time constant of ~6 min at room temperature (Steyer et al., 1997).

Fig. 8 shows an example from a cell observed after a 2-min period of stimulation by elevated external $[K^+]$. Fig. 8 *A* plots fluorescence at the site of an appearing granule. As the granule appeared (*filled circles*), fluorescence rose. Fluorescence reached a plateau, presumably because the granule reached the plasma membrane (*open circles*). Coordinates in the plane of the membrane were determined as in Fig. 5, and the resulting trajectory is plotted in Fig. 8 *B*. In Fig. 8 *C*, we assumed that the granule had reached the plasma membrane when fluorescence reached a plateau and used the curve in Fig. 2 *H* (*continuous curve*) to calculate the granule's vertical position from its intensity. The continuous curve in Fig. 2 *H* is more appropriate than the dashed one used in an earlier analysis (Steyer et al., 1997), because it is based on a calibration procedure that includes cytosol. The vertical coordinates are then plotted against the horizontal movement of the granule in the direction of its largest displacement.

Fig. 8 *D* plots four trajectories comparable to that of Fig. 8 *C*. The granules yielding the two uppermost trajectories ultimately performed exocytosis. That on the lower left detached from the plasma membrane and ascended back into the cytosol, and that on the lower right was near the plasma membrane from the beginning but left the plasma membrane during stimulation.

All granules in Fig. 8, *C* and *D*, approached the plasma membrane at an angle. Their approach trajectories often seem directed rather than random, as if they marked the presence of tracks or filaments whereupon the granules moved. In seven approach trajectories measured in three dimensions, granules approached at an average velocity of

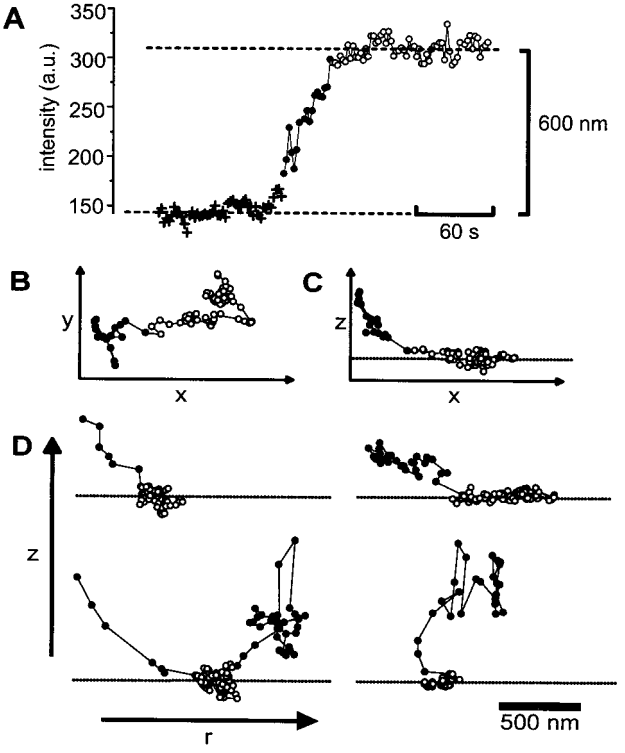

FIGURE 8 Granules approaching and leaving the plasma membrane. Granule positions were recorded in normal buffer after 2 min in stimulation buffer plus 10 μM nicotine. The stimulation buffer caused exocytosis that partially depleted the plasma membrane of granules. Under this experimental condition, new granules slowly appear as they approach the plasma membrane from the cytosol (Steyer et al., 1997). (*A*) Fluorescence intensity at the site of an appearing granule, both before (+) and after (●,○) the granule became visible. – – –: (*Lower*) Fluorescence background calculated as the average of the crosses. (*Upper*) Plateau value calculated from the average of all but the first five open circles. Open circles replace filled circles after the fluorescence of the granule had first exceeded 90% of its plateau value. The distance calibration on the right is approximate (see Fig. 2 *H*, *continuous curve*) and assumes that the granule had reached the plasma membrane when its brightness reached a plateau. The time interval between consecutive image frames was 2 s. (*B*) Trajectory of the granule in the plane of the membrane. Coordinates were determined as in Fig. 4 and are plotted at 2-s intervals. (*C*) Vertical distance (z) from the plasma membrane, assuming the granule reached the plasma membrane when its brightness reached the plateau level. z was calculated from Fig. 2 *H* (defined by two *continuous lines*). The abscissa (r) represents the direction of the granules' largest lateral displacement. – – –, Plateau level in *A*. For distance calibration see the bottom of *D*. (*D*) Vertical distance against r as in *C*, but on four other granules from different cells. Dashed lines were obtained as in *C*. (*Upper*) Two granules that underwent exocytosis during a second application of elevated [K^+]. (*Lower left*) A granule that approached the plasma membrane from the left and left to the right. (*Lower right*) A granule leaving the plasma membrane after a period of continuous presence; the recording was made during a first period of stimulation. The calibration bar refers to all panels except *A*. Data acquisition with a slow-scan CCD camera (see Materials and Methods). We analyzed seven cells and found 23 granules showing strong changes in fluorescence, indicating vertical movement. For our vertical calibration to be applied, the granule must be docked to the plasma membrane at one time and be absent at another. We believe this was true for seven granules. Some underwent exocytosis. Others appeared at the plasma membrane and then docked, as judged by an increase in fluorescence followed by a plateau, and two granules docked and then detached, as suggested by a plateau in fluorescence followed by a decrease. We required that the plateau period contained at least 60 s, where the rms fluctuations in fluorescence remained at <10% of the intensity change caused by the appearing or departing granule. Of the seven granules, one was not plotted because it approached the plasma membrane within a single sampling interval, and another was not because it was visible from the beginning and did not approach the membrane from a distance sufficient to define the angle of approach.

42 ± 8 nm/s. Their top speed over a 2-s interval was 137 ± 18 nm and might approach that of actin-mediated transport of organelles in neuronal growth cones if measured at a higher temperature (480 nm/s at 37°C; Evans and Bridgman, 1995).

DISCUSSION

Evanescent-field microscopy by epiillumination

We have used total internal reflection to set up an evanescent field within a thin region of cytosol where cells adhere to a glass coverslip. Like Stout and Axelrod (1989) and Conibear and Bagshaw (1996), we used a high numerical aperture objective both to generate the evanescent field and to observe the fluorescence excited by it. In a cell several microns thick, the method is effective in avoiding out-of-focus fluorescence and hence in imaging submembrane particles at the full resolution afforded by a NA 1.4 objective. We now discuss the strengths and weaknesses of this approach as compared to the more conventional method of generating evanescent fields with a prism.

The main disadvantage compared to prism methods is the difficulty of controlling the angle of incidence at the glass/cytosol interface, and hence the depth of penetration of the evanescent field. Generating an evanescent field by epiillumination relies on the difference between the numerical aperture and the refractive index of the illuminated medium. The highest numerical aperture available in commercial objectives is 1.4, with the exception of a recently introduced objective having a NA of 1.65 (APO 100 × O HR, Olympus, Japan). The refractive index of water is 1.33, and the refractive index of cytosol is given as 1.36–1.37 (Bereiter-Hahn et al., 1979). In a NA 1.4 objective, even those rays that pass the most peripheral region of the back focal plane barely surpass the critical angle for total internal reflection in cytosol. We held fluorescent beads at varying distances from the interface and measured the distance over which their fluorescence intensity declines e-fold (space constant). In saline plus bovine serum albumin, the space constant is ~185 nm, whereas in the cytosol of PC-12 cells it is ~640 nm. Because the field is barely evanescent in cytosol, the resolution in the vertical direction is mostly due to the small focal depth of the objective. Some evanescent light might even become propagated when reflected by large cytosolic particles such as granules or mitochondria. Nonetheless the method is a clear improvement over epifluorescence, as it does resolve single granules beneath the plasma membrane. Smaller and better controlled penetration depths will require objectives of higher numerical aperture than 1.4.

The advantages of epiillumination all follow from observing the specimen from the side on which the evanescent field is generated. First, the light collection efficiency is higher, as significantly more than half of the fluorescence originating from within the evanescent field radiates toward the side of higher refractive index (Axelrod et al., 1992). Second, because fluorescent structures are viewed directly and not through a layer of water and through the cell itself, one may use oil immersion objectives with their high numerical aperture and avoid the image degradation possibly caused by intracellular refracting structures such as granules. Third, one may imagine the dual use of objectives as a laser light trap combined with evanescent-field imaging of single molecules. Finally, epiillumination provides unrestricted access to one side of the specimen. It allows the use of patch clamps and other microdevices for electrical recording, as well as cantilevers in atomic force microscopy.

Motion of granules beneath the plasma membrane

Granules wander randomly around a resting position but otherwise move only a little. This behavior could be modeled quantitatively by assuming granules to be held on a 70-nm-long tether, or to be imprisoned in a cage with a radius 70 nm larger than that of a granule. Indeed, deep-etch electron micrographs do show chromaffin granules tethered to the cytoskeleton, and a filamentous actin meshwork beneath the plasmalemma of chromaffin cells (actin cortex) seems to surround a granule like a cage (Nakata and Hirokawa, 1992). We view our result as direct evidence that the movement of granules near the plasma membrane is restricted by a meshwork, as has been postulated by others (Trifaró and Vitale, 1993). Within the reach of the cage or the tether, granules diffused with a diffusion coefficient of 19×10^{-4} $\mu m^2/s$ in our measurements.

For the vast majority of granules, movement over longer distances was slow and apparently random, with a diffusion coefficient of about $D = 2.0 \times 10^{-4}$ $\mu m^2/s$. This is roughly consistent with an earlier estimate that lumped together slow and rapid diffusion over 8 s (3×10^{-4} $\mu m^2/s$; Steyer et al., 1997). At $D = 2.0 \times 10^{-4}$ $\mu m^2/s$, a granule would move an average distance of 28 nm in 1 s, 0.54 μm in 6 min, and 1.7 μm in 1 h. According to Stokes' law, a sphere with the diameter of an average chromaffin granule (330 nm; Parsons et al., 1995; Plattner et al., 1997) would diffuse at $D = 1.47$ $\mu m^2/s$ in aqueous medium with a viscosity of 0.851×10^{-3} Ns/m^2. This is ~7000-fold faster than the diffusion of granules beneath the plasma membrane. Clearly granules experience significant drag when they move.

Morphology suggests the actin cortex as a major source of drag (Nakata and Hirokawa, 1992). When stimulation raises cytosolic $[Ca^{2+}]$, Ca^{2+} apparently activates actin-severing enzymes and thereby thins the actin cortex (Trifaró and Vitale, 1993, but see also Nakata and Hirokawa, 1992). When testing whether granules are liberated from their constraints during stimulation, we found that the diffusion coefficient barely doubled. An increase with stimulation would be consistent with the idea that the actin cortex exerts drag on granules.

Do granules move actively?

The lateral movement of most membrane-resident granules seems random rather than directed; otherwise the MSD plots in Figs. 5 and 6 would curve upward (Qian et al., 1991; Saxton and Jacobson, 1997). Rarely, granules are seen to wander in a directed fashion over micron distances in resting chromaffin cells. Such movements, although not analyzed here, could not be diffusive and presumably consume energy. The same applies after stimulation, where approaching granules frequently move over near-micron distances in a seemingly directed fashion (Fig. 8). In permeabilized PC-12 cells containing granules labeled with green fluorescent protein, such long-distance motion is abolished when MgATP is removed from the cytosol and is almost certainly mediated by actin filaments (Th. Lang, personal communication). It is tempting to speculate that the movements in Fig. 8 arise similarly.

Recent studies have shown that a small subset of secretory vesicles is preferentially released during a brief stimulus, in both endocrine cells (Thomas et al., 1993; Heinemann et al., 1994; Moser and Neher, 1997) and neurons (Stevens and Tsujimoto, 1995). The pool of readily releasable vesicles is replenished with time constants of ~10 s in both cell types (Stevens and Tsujimoto, 1995; Moser and Neher, 1997). Does this replenishment reflect the movement of fresh granules toward the plasma membrane, or the awakening of dormant granules that were already docked? For endocrine cells, recent evidence supports the second alternative. Electron microscopic studies on chromaffin (Parsons et al., 1995; Steyer et al., 1997; Plattner et al., 1997) and pituitary cells (Parsons et al., 1995) show more granules bound to the plasma membrane than are rapidly releasable, and video microscopy has shown that new granules take hundreds rather than tens of seconds to reach the plasma membrane (Steyer et al., 1997). The present results add to this evidence. If transport to the plasma membrane is active, it will require MgATP. Because the readily releasable pool can be released in the absence of MgATP (Thomas et al., 1993; Heinemann et al., 1994; Parsons et al., 1995), it can probably be replenished without the docking of new granules.

Lateral mobility and docking

Many of the granules observed here were most likely bound to the plasma membrane or docked (Steyer et al., 1997). Does docking contribute to the drag on the movement of granules? The lateral mobility of granules diminishes by only about fivefold when granules contact the plasma membrane (Steyer et al., 1997), suggesting that the plasma mem-

brane is not the main source of drag. Indeed, lipid bilayers on their own are too fluid to exert significant drag; rhodopsin, for example, has seven transmembrane domains and diffuses at $D = 4000 \times 10^{-4}$ $\mu m^2/s$ in the membrane of rod outer segment disks (Poo and Cone, 1974). In the plasma membrane of differentiated cells, proteins diffuse more slowly, with rates varying from 100×10^{-4} $\mu m^2/s$ to unmeasurably low (Jacobson et al., 1987). Slowed diffusion in the plasma membrane is thought to arise through interaction with elements of the cytoskeleton. It is likely that any drag on granules while they are bound to a docking site will also be due, at least indirectly, to the cytoskeleton.

However slow, the lateral motion of granules can make it difficult to recognize whether successive granules undergoing exocytosis use the same docking site. A vacant site will diffuse at a minimum of 2×10^{-4} $\mu m^2/s$, the diffusion coefficient of a docking site with a granule attached. Therefore, during the 6 min an average cytosolic granule spends in reaching the plasma membrane (Steyer et al., 1997), the site would diffuse 0.5 μm^2. If 1.3 granules/μm^2 are arranged in a square grid on the plasma membrane, the average distance between subsurface granules is 0.88 μm, not much more than the distance covered by a docking site while it is vacant. Hence an empty docking site will probably not be filled again before it has diffused far enough to meet or even pass another granule.

We thank J. Pauli for building critical mechanical components, I. Wunderlich for chromaffin cells, and Th. Lang for suggestions on the manuscript.

This work was supported by the Max Planck Society.

REFERENCES

Axelrod, D., E. H. Hellen, and R. M. Fulbright. 1992. Total internal reflection fluorescence. *In* Fluorescence Spectroscopy: Principles and Applications, Vol. 3: Biochemical Applications. J. Lakowicz, editor. Plenum Press, New York.

Bereiter-Hahn, J., C. H. Fox, and B. Thorell. 1979. Quantitative reflection contrast microscopy of living cells. *J. Cell Biol.* 82:767–779.

Betz, W. J., and J. K. Angleson. 1998. The synaptic vesicle cycle. *Annu. Rev. Physiol.* 60:347–363.

Bi, G.-Q., R. L. Morris, G. Liao, J. M. Alderton, J. M. Scholey, and Steinhart. 1997. Kinesin- and myosin-driven steps of vesicle recruitment for Ca^{2+}-regulated exocytosis. *J. Cell Biol.* 138:999–1008.

Conibear, P. B., and C. R. Bagshaw. 1996. Measurement of nucleotide exchange kinetics with isolated synthetic myosin filaments using flash photolysis. *FEBS Lett.* 380:3–16.

Evans, L. L., and P. C. Bridgman. 1995. Particles move along actin filament bundles in nerve growth cones. *Proc. Natl. Acad. Sci. USA.* 92:10954–10958.

Ghosh, R. N., and W. W. Webb. 1994. Automated detection and tracking of individual and clustered cell surface low density lipoprotein receptor molecules. *Biophys. J.* 66:1301–1318.

Heinemann, C., R. H. Chow, E. Neher, and R. S. Zucker. 1994. Kinetics of the secretory response in bovine chromaffin cells following flash photolysis of caged Ca^{2+}. *Biophys. J.* 67:2546–2557.

Jacobson, K., A. Ishihara, and R. Inman. 1987. Lateral diffusion of proteins in membranes. *Annu. Rev. Physiol.* 49:163–175.

Kao, H. P., and A. S. Verkman. 1994. Tracking of single fluorescent particles in three dimensions: use of cylindrical optics to encode particle position. *Biophys. J.* 67:1291–1300.

Kumakura, K., K. Sasaki, T. Sakurai, M. Ohara-Imaizumi, H. Misonon, S. Nakamura, Y. Matsuda, and Y. Nonomura. 1994. Essential role of myosin light chain kinase in the mechanism for MgATP-dependent priming of exocytosis in adrenal chromaffin cells. *J. Neurosci.* 14: 7695–7703.

Kusumi, A., S. Yasushi, and M. Yamamoto. 1993. Confined lateral diffusion of membrane receptors as studied by single particle tracking (nanovid microscopy). Effects of calcium-induced differentiation in cultured epithelial cells. *Biophys. J.* 65:2021–2040.

Lang, T., I. Wacker, J. Steyer, C. Kaether, I. Wunderlich, T. Soldati, H.-H. Gerdes, and W. Almers. 1997. Ca^{2+}-triggered peptide secretion in single cells imaged with green fluorescent protein and evanescent-wave microscopy. *Neuron.* 18:857–863.

Majlof, L., and P.-O. Forsgren. 1993. Confocal microscopy: important considerations for accurate imaging. *Methods Cell Biol.* 38:79–95.

Miyamoto, S., T. Funatsu, S. Ishiwata, and S. Fujime. 1993. Changes in mobility of chromaffin granules in actin network with its assembly and Ca^{2+}-dependent disassembly by gelsolin. *Biophys. J.* 64:1139–1149.

Moser, T., and Neher, E. 1997. Rapid exocytosis in single chromaffin cells recorded from mouse adrenal slices. *J. Neurosci.* 17:2314–2323.

Nakata, T., and N. Hirokawa. 1992. Organization of cortical cytoskeleton of cultured chromaffin cells and involvement in secretion as revealed by quick-freeze, deep-etching, and double-label immunoelectron microscopy. *J. Neurosci.* 12:2186–2197.

Oheim, M., D. Loerke, W. Stühmer, and R. H. Chow. 1998. The last few milliseconds in the life of a secretory granule: docking, dynamics and fusion visualized by total internal reflection microscopy (TIRFM). *Eur. Biophys J.* 27:83–98.

Parsons, T. D., J. R. Coorssen, H. Horstmann, and W. Almers. 1995. Docked granules, the exocytic burst, and the need for ATP hydrolysis in endocrine cells. *Neuron.* 15:1085–1096.

Plattner, H., A. R. Artalejo, and E. Neher. 1997. Ultrastructural organization of bovine chromaffin cell cortex—analysis by cryofixation and morphometry of aspects pertinent to exocytosis. *J. Cell Biol.* 139:1709–1717.

Poo, M. M., and R. A. Cone. 1974. Lateral diffusion of rhodopsin in the photoreceptor membrane. *Nature.* 247:438–441.

Qian, H., M. P. Sheetz, and E. L. Elson. 1991. Single particle tracking (analysis of diffusion and flow in two-dimensional systems). *Biophys. J.* 60:910–921.

Saxton, M. J. 1993. Lateral diffusion in an archipelago (single-particle diffusion). *Biophys. J.* 64:1766–1780.

Saxton, M. J., and K. Jacobson. 1997. Single-particle tracking: applications to membrane dynamics. *Annu. Rev. Biophys. Biomol. Struct.* 26: 373–399.

Smith, C. B., and W. J. Betz. 1996. Simultaneous independent measurement of endo- and exocytosis. *Nature.* 380:531–534.

Stevens, C. F., and T. Tsujimoto. 1995. Estimates for the pool size of releasable quanta at a single central synapse and for the time required to refill the pool. *Proc. Natl. Acad. Sci. USA.* 92:846–849.

Steyer, J. A., H. Horstmann, and W. Almers. 1997. Transport, docking and exocytosis of single secretory granules in live chromaffin cells. *Nature.* 388:474–478.

Stout, A. L., and D. Axelrod. 1989. Evanescent field excitation of fluorescence by epi-illumination microscopy. *Appl. Opt.* 28:5237–5242.

Terakawa, S., J. H. Fan, K. Kumakura, and M. Ohara-Imaizumi. 1991. Quantitative analysis of exocytosis directly visualized in living chromaffin cells. *Neurosci. Lett.* 123:82–86.

Terrian, R., and D. Prekeris. 1997. Brain myosin V is a synaptic vesicle-associated motor protein: evidence for a Ca^{2+}-dependent interaction with the synaptobrevin-synaptophysin complex. *J. Cell Biol.* 137:1589–1601.

Thomas, P., J. G. Wong, A. K. Lee, and W. Almers. 1993. A low affinity Ca^{2+} receptor controls the final steps in peptide secretion from pituitary melanotrophs. *Neuron.* 11:93–104.

Trifaró, J. M., and M. L. Vitale. 1993. Cytoskeleton dynamics during neurotransmitter release. *Trends Neurosci.* 16:466–472.